Original paper

The effect of attenuation map, scatter energy window width, and volume of interest on the calibration factor calculation in quantitative ^{177}Lu SPECT imaging: Simulation and phantom study

Elham Karimi Ghodoosi[a, b, *]

elham.karimi@helmholtz-muenchen.de

Calogero D'Alessandria[b]

Ye Li[c]

Alexandra Bartel[b]

Markus Köhner[b]

Vera Höllriegl[a]

Nassir Navab[e]

Matthias Eiber[b]

Wei Bo Li[a, *]

wli@helmholtz-muenchen.de

Eric Frey[d]

Sibylle Ziegler[b, f]

[a]Institute of Radiation Protection, Helmholtz Zentrum München, German Research Center for Environmental Health, Ingolstädter Landstraße 1, 85764 Neuherberg, Germany

[b]Nuklearmedizinische Klinik und Poliklinik, Klinikum Rechts der Isar, Technische Universität München, 81675 Munich, Germany

[c]Department of Electrical and Computer Engineering, Whiting School of Engineering, Johns Hopkins University, Baltimore, MD 21218, United States

[d]The Russell H Morgan Department of Radiology and Radiological Science, School of Medicine, Johns Hopkins University, Baltimore, MD 21287, United States

[e]Computer Faculty, Computer Aided Medical Procedures, Technische Universität München, Boltzmannstr. 3, 85748 Garching, Germany

[f]Department of Nuclear Medicine, University Hospital of LMU Munich, Marchioninistr. 15, 81377 Munich, Germany

*Corresponding authors at: Institute of Radiation Protection, Helmholtz Zentrum München, German Research Center for Environmental Health (GmbH), Ingolstädter Landstraße 1, 85764 Neuherberg, Germany.

Abstract

Purpose

The objective of this study was to evaluate the image degrading factors in quantitative ^{177}Lu SPECT imaging when using both main gamma photopeak energies.

Methods

Phantom measurements with two different vials containing various calibrated activities in air or water were performed to derive a mean calibration factor (CF) for large and small volumes of interest (VOIs). In addition, Monte Carlo simulations were utilized to investigate the effect of scatter energy window width, scatter correction method, such as effective scatter source estimation (ESSE) and triple energy window (TEW), and attenuation map on the quantification of ^{177}Lu. Results: The measured mean CF using large and small VOIs in water was 4.50 ± 0.80 and 4.80 ± 0.72 cps MBq^{-1}, respectively. Simulations showed a reference CF of 3.3 cps MBq^{-1} for the water-filled phantom considering all photons excluding scattered events. By using the attenuation map

generated for 190 keV photons, the calculated CFs for 113 keV and 208 keV are 10% lower than by using the weighted mean energy of 175 keV for [177]Lu. The calculated CF using the TEW correction was 17% higher than using the ESSE method for a water-filled phantom. However, our findings showed that an appropriate scatter window combination can reduce this difference between TEW and ESSE methods.

Conclusions

The present work implies that choosing a suitable width of scatter energy windows can reduce uncertainties in radioactivity quantification. It is suggested to generate the attenuation map at 113 keV and 208 keV, separately. Furthermore, using small VOIs is suggested in CF calculation.

Keywords: [177]Lu; SPECT/CT; Scatter window; Scatter fraction; Attenuation map; Calibration factor

1 Introduction

A number of ^{177}Lu-labeled peptides for targeting prostate cancer like ^{177}Lu-labeled RGD-BBN heterodimeric peptide, ^{177}Lu-labeled GRP-R Agonist, and ^{177}Lu-labeled PSMA I&T (I&T for imaging and therapy) was recently investigated [1–4]. [177]Lu is a beta emitter and is used for radionuclide therapy. In addition, it emits gamma rays which can be detected by SPECT/CT for imaging the distribution of ^{177}Lu over time in tumors or other organs and further for estimating the absorbed doses of individual organs [5,6]. In quantitative SPECT imaging, a calibration factor (CF) is required to convert obtained counts to radioactivity. This factor depends on the type of collimator, the sensitivity of the camera for the applied energy windows, and the effects of attenuation and scatter. Since ^{177}Lu has two gamma photopeaks in its energy spectrum, the image acquisition and reconstruction parameters depend on the choice of primary energy windows.

Protocols for ^{177}Lu targeted therapy were reported by the Medical Internal Radiation Dose (MIRD) Committee of the Society of Nuclear Medicine and the International Atomic Energy Agency [6–8]. The MIRD committee emphasized in pamphlet No. 23 that during the calibration phantom measurement, the experimental conditions should be close to the clinical setting representing the attenuation and scattering situation [6]. Recently, the MIRD committee suggested in pamphlet No. 26, that the use of medium energy collimator for both gamma photopeak energies is suitable. The authors suggested 20% and 15% width for the main energy windows (centered on the photopeak energy) for 208 and 113 keV, respectively. It is concluded that the ratio of scattered photons to total photons acquired for the 113 keV energy window is much higher than for the 208 keV energy window [8].

CF calculated based on reconstruction parameters, e.g. the attenuation correction, scatter correction (SC) and collimator detector response (CDR) compensation, were previously investigated [5,7–23]. Sanders et al. [5] used different spheres with different volumes (0.5 ml–16 ml) considering both photopeak energies of [177]Lu (208 keV and 113 keV) and demonstrated that the sensitivity depends on the choice of the photopeak window, with a higher sensitivity in the lower photopeak energy. Sandström et al. [14] calculated the sensitivity factor using an elliptical water phantom including a spherical source with 100 ml volume containing 1 GBq of ^{177}Lu and concluded that the small VOI method can reduce the partial volume effect. Hippeläinen et al. [15] studied the effect of compensation methods on the recovery coefficient (RC) using the high photopeak energy of [177]Lu. They applied different combinations of correction methods and concluded that by applying the collimator detector response (CDR) compensation, RC is intensely improved compared with applying only the attenuation correction (AC). Moreover, Mezzenga et al. [22] investigated the correlation between the object size, 3D-OSEM algorithm, and the image noise. To improve the calibration accuracy, they suggested a large uniform phantom should be used as a reference geometry. D'Arienzo et al. [16,23] suggested that using the 208 keV photopeak energy of ^{177}Lu could result in sufficient accuracy of CF [16]. They validated using transmission-dependent convolution subtraction correction algorithm for scattering correction [23]. Nijs et al. [13] applied the triple energy window (TEW) method and reported that the TEW is noise sensitive and the use of wider windows is more stable. It was shown that using the effective scatter source estimation (ESSE) and both gamma photopeak energy windows results in a better SC. Furthermore, Uribe et al. [17] applied the TEW and the analytical photon distribution interpolated (APDI) techniques as two different SC methods and found that in absence of background, the TEW technique causes under/overestimation of the activity for small/large spheres and recommended the APDI SC method for lesions in non-uniform attenuation areas.

In addition to the experimental measurements, Monte Carlo simulations are used to validate quantitative SPECT/CT imaging, to evaluate the sensitivity of modelling, to optimize acquisition parameters, and to estimate the 3D distribution of radioactivity in organs [24–30]. Physical factors such as CDR, attenuation and scatter compensation can be studied by modeling their effects in the reconstruction algorithm [31,32]. Uribe et al. [29], by using GATE, modeled the physics of the bremsstrahlung emissions of ^{177}Lu within a cylinder phantom. They showed negligible contribution of these photons to the final image. Moreover, Costa et al. [30] evaluated and proposed three methods to reduce simulation time with GATE. Among the various open source codes for simulation, the Monte Carlo simulation code SIMIND [33] is used for standard clinical SPECT cameras.

Besides the simulation and the phantom studies, the impact of image quality and image registration on the image-based dosimetry has also investigated in a number of publications. For instance, Grassi et al. [34] showed the effect of the applied registration algorithm on the dosimetry calculations, and suggested using deformable image registration in clinical practice.

The activity quantification of ^{177}Lu was mostly studied for the higher gamma photopeak energy and only up to two different scatter energy window (SW) widths have been applied in previous studies. In addition, the effect of SW width on the CF for both gamma photopeak energies has not yet been investigated. Moreover, the influence of the attenuation map on the CF was not yet evaluated numerically for the weighted energy of ^{177}Lu and each of the main gamma photopeak energies. In many implementations, only the TEW method is offered for SC. Therefore, in the present work, by applying SIMIND, the effect of scatter energy window widths, SC method, and attenuation map at four energies (113, 175, 190, and 208 keV) was investigated on the CF calculation. To investigate the impact of object size and VOI definition on SPECT image data of ^{177}Lu, phantom measurements were performed and the CF was calculated. Both photopeak energies were applied for simulations and experimental measurements.

2 Materials and methods

2.1 Phantoms

In this work, a NEMA IEC body phantom (Model PET/IEC-BODY/P) [35] was used with 9.7 l capacity as a body. Two different vials, one of a medium volume (180 ml) and one small volume (25 ml), were inserted to represent a kidney and a lesion, respectively (Fig. 1). For each measurement, the position of the vial inside the phantom was chosen to ensure the same geometrical imaging situation relative to the camera head. The vial with medium volume was an oval shaped bottle with 8 cm height (wall thickness 0.04 cm), and the small one was a cylinder with 5 cm height and 3.2 cm diameter. This specific volume of 180 ml was chosen because the average volume of a kidney measured from six patient CT data sets was 180 ± 26.5 ml. The phantom was either filled with water or air, and the small or the medium vial was fixed to the bottom of the phantom. To study the influence of the activity concentration of the source vials on the CF, the calibration process was repeated seven times with 5 different activities of ^{177}Lu (Table 1). Two measurements were performed with activity concentration ratios of 1:70 and 1:68 between background and vial. Activity was measured with a Capintec CRC-15R Dose Calibrator (Pittsburgh, PA).

Fig. 1 Siemens Symbia T6 SPECT-CT with NEMA IEC body phantom filled with water including a vial with 25 ml volume (calibrated activity of 651 MBq).

Table 1 Configuration of the phantom measurements and ^{177}Lu activities inside the vials used for the CF calculation (distinct CF calculation was performed for each of the photopeak energy windows).

Phantom measurement	NEMA IEC Phantom medium	Vial volume (ml)	Calibrated activity inside the vial at the time of measurement (MBq)	Activity concentration (MBq ml^{-1})	Calibrated activity in phantom (background) (MBq)
A	Air	25	641.3	25.7	NA
B	Water	25	641.3	25.7	0
C	Water	25	72.5	2.9	0
D	Water	25	32.4	1.3	0
E	Water	180	437.2	2.4	0
F	Water	180	437.2	2.4	1:70
G	Water (see F, after 7 days)	180	234.5	1.3	1:68

NA: Not Applicable.

2.1.1 Data acquisitions

All acquisitions were performed on a SIEMENS SPECT/CT (SYMBIA T6) at the Nuclear Medicine Department of Klinikum Rechts der Isar, TU Munich, Germany with a medium energy collimator. The main parameters of the clinical settings for SPECT acquisition and image reconstruction can be found in Table 2. The images were reconstructed by an ordered subset expectation maximization (OSEM) algorithm [31] which was implemented by the vendor (Siemens Healthcare), and CDR compensation was included in the OSEM algorithm [36]. Attenuation correction was performed based on CT images and the attenuation map was created for a gamma energy of 190 keV (^{81}Kr in vendor software). The TEW correction method [32] was applied for the two main gamma photopeak energy windows of ^{177}Lu: 113 keV and 208 keV.

Table 2 SPECT acquisition and reconstruction parameters (clinical settings).

Acquisition	
Collimator	ME
Matrix	128 × 128
Scan arc (°)	180
Number of projections	90
Pixel size (mm²)	4.8 × 4.8
Dwell time (s̶e̶e̶)	10
Photopeak main energy windows: Photopeak 1, Photopeak 2	113 keV ± 10% width, 208 keV ± 6% width
Scatter energy windows (SWs): Photopeak 1, Photopeak 2	92.4 keV ± 10% width (LSW)[a], 131.6 keV ± 6.5% width (USW)[b], 183.6 keV ± 6.2% width (LSW), 230.8 keV ± 4.5% width (USW)
Reconstruction	
Method	Flash 3D (Siemens)
Corrections	AC, SC (TEW), and CDR
Iteration/Subsets	15i/8ss
Transverse reconstructed matrix	128 × 128
Filter post reconstruction	Gaussian 12 mm

(LSW)[a]: lower scatter window; (USW)[b]: upper scatter window.

2.1.2 Determination of calibration factor in measurements

The total counts are normally obtained from a VOI defined in the images. Then the CF expressed in units of counts per second (cps) per MBq can be calculated as:

$$CF\ (cps/MBq) = \frac{C}{A} \tag{1}$$

where C is the total count rate within the VOI in the images (cps); A is the calibrated activity (MBq) at the measurement time within the individual VOI (large, small).

In our measurements, the VOIs were delineated in two ways: (1) A large volume which covered the known geometrical size of each vial; and (2) A small spherical volume at the center of each vial (i.e. 15% volume of each vial: 3.75 ml for small vial and 27 ml for medium one) to reduce the influence of the partial volume effect at the edge of the vial [37]. The value of count rates found in the large and small volume is denoted as C_L and C_S in the following:

C_L = Total count rate inside the large VOI covering the whole organ, and

C_S = Maximum count rate found within the small VOI × number of voxels within the small VOI.

The VOI was defined by using PMOD software (PMOD Technologies LLC, Zurich). For each of the photopeak energy windows and for the medium and small vial, the CF was calculated, independently, resulting in 14 values of CF for small and large VOIs, separately. Afterwards, by using the results of phantom measurements in water as listed in Table 1 (B–G), a mean calibration factor (mCF) for large and small VOIs was calculated and the relative uncertainty (D%) of mCF was calculated as a ratio of the difference between calibrated activity and measured activity using:

$$D\% = \frac{Calibrated\ activity\ (MBq) -\ Measured\ activity\ using\ mCF\ (MBq)}{Calibrated\ activity\ \ (MBq)} \times 100 \tag{2}$$

The activity is the activity in the used volume of interest.

2.2 Monte Carlo simulations

In this work, the Monte Carlo simulation code SIMIND [18] was utilized to generate source distributions which are similar to our phantom measurements and to analyze the factors affecting reproducibility of the CF. In the simulation, a 9.7 l cylinder phantom containing a 25 ml vial with 650 MBq of ^{177}Lu was used. To cover the principal energies needed for imaging, the full energy spectrum of ^{177}Lu from 54 keV to 250 keV was used in the simulation. In addition, a NaI(Tl) crystal with 1.54 cm thickness and a medium energy collimator were used in the simulation to mimic the detector. The energy resolution of the gamma camera was set to 9% FWHM at 140 keV, and the number of simulated projections was set to 128 in a 360° full rotation mode. All images were reconstructed by using the OSEM algorithm which including the CDR function, AC and SC as in the experimental study.

A full CDR function was generated by simulating a point source in various distances from the surface of the collimator (2, 5, 10, 15, 20, 30, 40, and 60 cm) using the clinical setting for the main photopeak energy windows of ^{177}Lu (113 keV with 20% width and 208 keV with 12% width). AC was performed by using an attenuation map derived from a CT study as suggested by the MIRD guideline [8]. Because the AC for ^{177}Lu depends on the scaling between transmission and emission energies, different attenuation maps were generated at 190 keV (which was used in the clinical setting as default energy), 113 keV, 208 keV, and at the weighted energy, i.e. 175 keV, of ^{177}Lu [38]. Calibration from Hounsfield units to attenuation coefficient was made by scaling the units related to the main photopeak energy and the phantom medium. For this purpose, a bilinear model that describes the linear attenuation coefficient conversion ratio for air-and-water and water-and-plexiglass was used [39]:

$$\mu_{air+water,E} = \frac{CT_{H.U} \times \left\{ \mu_{water,E} - \mu_{air,E} \right\}}{1000} \tag{3}$$

$$\mu_{water+plexiglass,E} = \mu_{water,E} + \frac{CT_{H.U} \times \mu_{water,E_{eff}} \times \left\{ \mu_{plexiglass,E} - \mu_{water,E} \right\}}{1000 \times \left\{ \mu_{plexiglass,E_{eff}} - \mu_{water,E_{eff}} \right\}} \tag{4}$$

where: $CT_{H.U}$ is the value of CT number in Hounsfield unit, μ (cm^{-1}) is the attenuation coefficient for emission energy (E), and E_{eff} s the effective x-ray photon energy.

In addition, the relative uncertainty of calculated CFs when applying the AC at the above mentioned energies were determined.

As a reference, a CF was calculated for simulations in which only non-scattered events were taken into account, and the AC was applied using an attenuation map at the energy of 190 keV. For estimating SC, the TEW correction for the relevant main energy windows was applied, or the effective scatter source estimation (ESSE). In order to use ESSE, two scatter kernels (normalized scatter kernel, and scatter attenuation coefficient kernel) as the pre-calculated point-spread functions were needed [27]. These kernels were computed by using the SIMIND code and were then combined for further use in image reconstruction.

In our simulation, various scatter windows were applied in addition to the main windows at 208 keV and 113 keV (see Table 4 in results section). The effect of the scatter window width on the TEW method was studied by varying the lower and upper scatter windows. To investigate the accuracy of the SC, for all combinations of scatter energy windows, the scatter fraction (SCF) was determined and compared to the actual scatter fraction (ASCF). The SCF was calculated for each of the scatter energy windows (Table 4) following MIRD No. 26 [8].

$$SCF = \frac{Total\ scattered\ photons\ estimated\ by\ the\ TEW}{Total\ photons\ in\ main\ energy\ window\ before\ any\ correction} \tag{5}$$

The ASCF was determined as following:

$$ASCF = \frac{Total\ scattered\ photons\ in\ the\ main\ energy\ window\ before\ any\ correction}{Total\ photons\ in\ main\ energy\ window\ before\ any\ correction} \tag{6}$$

3 Results

3.1 Phantom measurements

The results of calculated CF_L in phantom measurements by using large VOIs in water with different activity concentrations in two volumes are shown in Fig. 2. For the 25 ml vial with varying activity concentrations (1.3, 2.9 and 26 MBq ml^{-1}), CF_L in water was about 1.50 ± 0.08 cps MBq^{-1} and 2.20 ± 0.10 cps MBq^{-1} for the 113 keV and the 208 keV photopeak energy, respectively. For the 180 ml vial with 1.3 and 2.4 MBq ml^{-1} activity concentrations, this factor was 2.30 ± 0.06 and 3.00 ± 0.10 cps MBq^{-1} for low and high photopeak energies (Fig. 2). By taking into account both photopeak energies, the calculated CF_L for the 180 ml vial was 37% higher than that for the 25 ml vial. The average mCF_L across energy windows and vial size was 4.50 ± 0.80 cps MBq^{-1}. The CF_L for the 25 ml and 180 ml vials with the same activity concentration (1.3 MBq ml^{-1}) showed the partial volume effect. By using the 180 ml vial only, the CF_L was higher compared to the small vial by 55% and 38% for 113 keV and 208 keV photopeak energies, respectively.
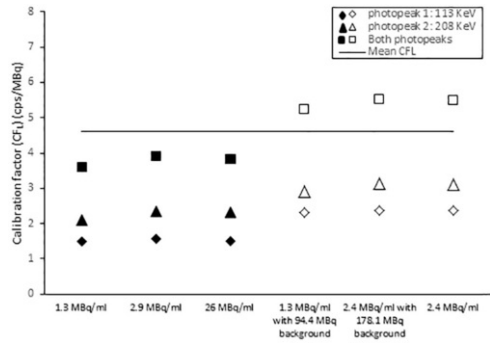
Fig. 2 The calculated calibration factor (CF_L) for six phantom measurements in water by using large volume of interest (VOI) for each photopeak energy windows with various activity concentrations of ^{177}Lu. Filled symbols: 25 ml vial representing a lesion. Open symbols: 180 ml vial representing a kidney. Black line: mean value of calibration factors (mCF_L) for all phantom measurements for both photopeak energies.

By using small VOIs, for the 25 ml vial, the CF_S was 1.60 ± 0.04 cps MBq^{-1} for the low photopeak energy and 2.50 ± 0.02 cps MBq^{-1} for the higher photopeak energy. The value of CF_{S} for the 180 ml vial was 2.30 ± 0.08 and 3.10 ± 0.01 cps MBq^{-1} for 113 and 208 keV photopeak energies, respectively. The mean CF_S (mCF_S) for 6 phantom measurements in water for both photopeak energies was 4.80 ± 0.72 cps MBq^{-1} (Fig. 3). It was observed, that for the same activity concentration, the calculated CF_S for the 180 ml vial were 32% and 26% higher than that for the small vial at the 113 and 208 keV photopeak energies, respectively.
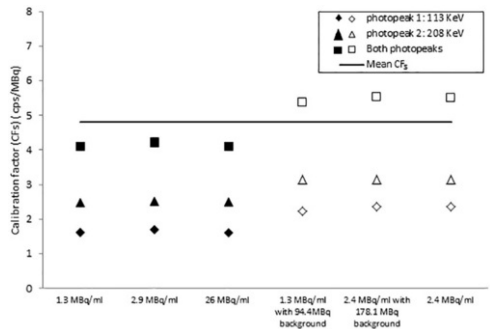
Fig. 3 The calculated calibration factor (CF_S) for six phantom measurements in water by using small volume of interest (VOI) for each photopeak energy windows with various activity concentrations of ^{177}Lu. Filled symbols: 25 ml vial representing a lesion. Open symbols: 180 ml vial representing a kidney. Black line: mean value of calibration factors (mCF_S) for all phantom measurements for both photopeak energies.

The results of activity quantification using a mean CF are shown in Table 3. For the large VOIs, the relative uncertainty of measured activity for the 25 ml and 180 ml vials (in the absence of the background) was −17.6% and +21%. However, by using the small VOIs, D was reduced to −7.8 and +6% for the 25 ml and 180 ml vials, respectively.

Table 3 Phantom quantification using mean calibration factor (mCF) based on two different VOI definitions.

Phantom measurement (refer to Table 1)	Calibrated activity at the time of measurement (MBq)	Measured activity (MBq) by SPECT using mCF from large VOI	Measured activity (MBq) by SPECT using mCF from small VOI
A	641.3	528.5 ($D = -17.6\%$)	591.37 ($D = -7.8\%$)
E	437.2	527.4 ($D = +21\%$)	463.48 ($D = +6\%$)

*D represents the difference of measured activity and calibrated activity.

Table 4 Simulation: scatter fraction (SCF) and calibration factor (CF) for different scatter energy windows (SWs).

Combination	Lower scatter window (keV)	Upper scatter window (keV)	SCF	CF

Scatter energy windows for the 113 keV photopeak energy				
1 (clinical setting)	84–100.8	123.2–140	0.29	1.90
2	84–100.8	123.2–175	0.28	2.00
3	74–100.8	123.2–140	0.42	1.70
4	74–100.8	123.2–150	0.39	1.80
5	74–100.8	123.2–170	0.29	2.00
6	54–100.8	123.2–133.2	0.43	1.70
7	54–100.8	123.2–170	0.30	1.80
8	54–100.8	123.2–140	0.43	1.70
9	90.8–100.8	123.2–133.2	0.29	2.00
Actual scatter fraction (ASCF): 0.66 CF reference: 1.37 cps MBq^{-1}				
Scatter energy windows for the 208 keV photopeak energy				
1 (clinical setting)	172.2–195	220.48–241.28	0.13	2.00
2	142–195	220.4–271.2	0.13	2.00
3	162–195	220.4–251.4	0.13	2.00
4	190–195	220.48–225.48	0.17	1.80
Actual scatter fraction (ASCF): 0.28 CF reference: 1.87 cps MBq^{-1}				

The width of the main photopeak energy window in all combinations was 100.8 keV–123.2 keV and 195 keV–220.4 keV for 113 and 208 keV photopeak energies, respectively.

3.2 SIMIND simulation results

AC, which was based on 175 and 190 keV instead of 113 keV, for the low photopeak energy, caused differences of −23% and −30% in CF calculation, respectively. For the high photopeak energy, this difference was 24% and 12% for 175 and 190 keV, respectively. The reference CF for the phantom filled with water considering all detected photons excluding scattered events, and the AC based on 190 keV was 3.30 cps MBq^{-1}. Using the ESSE method applied to all detected photons, the CF in water and air were 3.40 and 3.20 cps MBq^{-1}, respectively. However by using TEW, the CF was 17% higher in the water-filled phantom (4.00 cps MBq^{-1}) and about 6% lower in air (3.00 cps MBq^{-1}) in comparison to the ESSE method (Fig. 4). In Table 4, for each photopeak, the calculated SCF and CF for each scatter energy windows are given. It was observed, that the clinical setting causes −56.1% and −54.8% inaccuracy in the scattered photon estimation, for the 113 and 208 keV photopeak, respectively. Our results showed that for the 113 keV photopeak, if the width of the LSW is about 3 times wider than the clinical setting, the inaccuracy will be reduced to −34%.
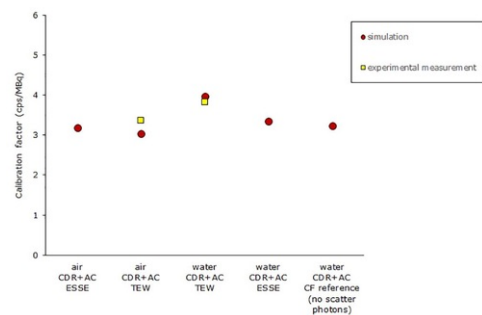
Fig. 4 Different scatter correction (SC) correction methods: the triple energy window (TEW) and effective scatter source estimation (ESSE) during simulation in water and air, compared to experimental measurements. The collimator detector response (CDR) and attenuation correction (AC) were applied in all simulations.

4 Discussion

As expected, it can be concluded that the calculated SPECT/CT CF depends on the object size, attenuation map, and choice of SW.

4.1 Calibration factor from phantom measurements

The results of our phantom measurements showed that different activity concentrations in the same volume of vials, with or without background, do not affect the CF (Figs. 2 and 3). However, there is a difference in the calculated CF_L and CF_S, using the same activity concentration for objects with different volumes. It was observed that for the vial with 180 ml volume, the CF_L and CF_S considering both photopeak energy contributions was 46 and 30% higher than for the small vial. This confirms the effect of object size on CF calculation, and hence on activity quantification.

It was observed, that compared to the small VOI, using a large VOI for calibration causes uncertainty of activity for a small or large object (see Table 3). Hence, it could be concluded that by using the small VOI, the effect of partial volume may be reduced compared to the large VOI. Dewaraja et al. [6] also described an underestimation of measured activities on a voxel level for small objects. Using the small VOI in the mCF_S will reduce the uncertainty in activity quantification and may be appropriate in patient studies, when organ volumes are known and homogenous activity distribution in the organ is assumed. It is thus suggested to draw a small volume within an organ with minimum volume of e.g. 4 mm^3, placed in an area of the organ without metastases. The total activity within the organ could be calculated as:

$$Activity\ within\ the\ small\ VOI\ (MBq) = CF_s^{-1}\left(\frac{MBq}{cps}\right) \times total\ count\ rate\ inside\ the\ small\ VOI\ of\ the\ organ\ (cps)$$

$$Total\ activity\ of\ the\ organ\ (MBq) = \frac{Activity\ within\ the\ small\ VOI\ (MBq) \times Total\ organ\ volume\ (ml)}{Volume\ of\ the\ small\ VOIs\ (ml)}$$

The total organ volume can be obtained from the CT images.

4.2 Calibration factor from simulations

The simulation showed that the attenuation map, the SC and the width of the SWs have a considerable effect on the accuracy of the calculated CF, which consequently results in over/underestimation of the measured activity. It was found that generating an individual attenuation map at each of the main gamma photopeak energies of ^{177}Lu may reduce the inaccuracy in CF. Furthermore, we found that a suitable scatter energy window width decreases the inaccuracy of the CF calculation. However, the ESSE technique may be a better alternative for SC.

The reference CF was about 15% lower than the CF_L calculated by the phantom measurements in water using the 25 ml vial (see Table 1: B). This difference may be related to differences in geometry and effective energy window in the simulation and measurements.

As expected, the attenuation correction showed a considerable dependence on the gamma energy, for which the attenuation map was created. The simulation results showed under/over-estimation in CF calculation by generating the attenuation map at 190 and 175 keV for low and high photopeak energy, correspondingly. The calculated CF for the 113 and 208 keV peak was about 7% and 12% smaller by applying the attenuation map generated at 190 keV, compared to using the attenuation map at 175 keV (^{177}Lu weighted energy). These differences are in line with the recommendation in MIRD pamphlet No.26 [8]. Thus, the implemented attenuation map at 190 keV (which is the default clinical setting) in the experimental measurement reduces the accuracy of CF calculation. Care should be taken to apply individual attenuation correction for each photopeak.

Considering the study by Sandström et al. [14], quantification problems in SPECT imaging mostly are related to AC and SC. For example, they showed the inevitable inaccuracy in the order of 10% due to the AC in experimental measurements. D'Arienzo et al. [16] analyzed four different reference conditions for gamma camera calibration. They showed that by using a well-calibrated field instrument, there is an uncertainty about 5% for gamma camera calibration factor.

Using ESSE as the SC method resulted in a CF closer to the CF reference value than using the TEW correction method (+6% vs +23%). The results are consistent with the result reported by de Nijs et al. [13]. They showed that both photopeak energies can be utilized when the ESSE correction technique is applied. In their experimental study, the difference between the calculated and the calibrated activity was less than 10%.Therefore, it may be concluded that applying the TEW correction may not exclude the scatter events sufficiently compared to the ESSE method and results in an inaccuracy of around 23% in quantitative activity measurements.

By using the best combination of the SW in this work, the scatter fractions (SCF) were closer to the related actual scatter fraction (ASCF) than using other SW combinations (Table 4), and were in the mentioned range in the MIRD pamphlet No. 26 [8]. The optimal SWs cause only 9% difference from the reference CF (3.3 cps MBq^{-1}). The results confirmed an improved SC by using the optimal combination. This showed that if TEW is applied, better SC can be achieved by adapting suitable SW widths, especially for the low photopeak energy.

The different SWs which were applied in the recently published quantitative phantom studies are shown in the Supplementary material. Robinson et al. [25], by using SWs with 3% width, concluded that applying TEW correction on SPECT images can cause significant inaccuracy in activity quantification. The simulation results confirmed the sufficiency of the USW width which is used in clinical applications. It may be concluded that the LSW for the low photopeak energy was broader than the USW due to the high background of scatter photons below 113 keV, which should be excluded from the detected photons. However, because of the contamination of main energy windows by downscattered photons which have at least 117 keV, the USW for low photopeak energy should not be wider than the MW width. It was observed that, using the abutting windows with the same width does not improve the scattered photons estimation and caused more inaccuracy in CF calculation. Thus, it may be concluded that the noise sensitivity of the LSW and USW is not the same.

The ideal SW width for the 208 keV photopeak was obtained by a smaller LSW and USW compared to the clinical setting (about 5 and 4 times smaller, respectively). The width of the SW for high photopeak energy influences the scatter contribution less than the SW of the lower photopeak, which is compatible with the findings of Delker et al. [11] and Uribe et al. [17] who considered the high photopeak energy of ^{177}Lu in their studies. Nijs et al. [13] concluded that TEW is noise sensitive and broader energy windows make this method much more stable for dynamic studies, however the results of this work confirm this only for LSW of the 113 keV peak. Although the noise sensitivity seemed to be negligible for the higher gamma photopeak energy in the current work, a narrower scatter energy window at 208 keV can reduce the bias in scatter estimation. Thus, in a setting, which does not offer ESSE, TEW correction could be used with SW widths shown in Table 2 in the Supplementary material.

5 Conclusion

In this work we showed that for improving quantitative ^{177}Lu SPECT imaging, the size of the calibration phantom should be considered at the calibration process. In addition, using a small volume of interest inside the phantom can be advantageous for determining the CF. The findings demonstrate a considerable influence of the attenuation map, SC method, and scatter window width on the SPECT/CT calibration reproducibility. Our results suggest that using ESSE as a SC can improve the activity estimation; however, as the TEW method is a widely accepted technique in clinical practice, a broader width for the LSW for the 113 keV photopeak energy may improve the accuracy of the activity quantification. Although the scatter estimate for the higher photopeak energy is not as sensitive to SW width as for the lower photopeak energy, a narrow SW can improve the calculated CF. Further evaluations will focus on optimizing scan and reconstruction parameters towards a clinically feasible, fast SPECT/CT protocol covering the whole body of the patient to estimate the dose of other organs at risk.

Funding

Acknowledgement

Appendix A. Supplementary data

Supplementary data to this article can be found online at https://doi.org/10.1016/j.ejmp.2018.11.009.

References

[1] D.L. Bailey, T.M. Hennessy, K.P. Willowson, E.C. Henry, D.L. Chan, A. Aslani, et al., In vivo quantification of ^{177}Lu with planar whole-body and SPECT/CT gamma camera imaging, *EJNMMI Phys* **2**, 2015, 20.

[2] L.E. Lantry, E. Cappelletti, M.E. Maddalena, J.S. Fox, W. Feng, J. Chen, et al., ^{177}Lu-AMBA: synthesis and characterization of a selective ^{177}Lu-labeled GRP-R agonist for systemic radiotherapy of prostate cancer, *J Nucl Med* **47**, 2006, 1144–1152.

[3] 1S. Okamoto, A. Thieme, J. Allmann, C. D'Alessandria, T. Maurer, M. Retz, et al., Radiation dosimetry for ^{177}Lu-PSMA I&T in metastatic castration-resistant prostate cancer: absorbed dose in normal organs and tumor lesions, *J Nucl Med* **58**, 2017, 445–450.

[4] L. Jiang, Z. Miao, H. Liu, G. Ren, A. Bao, C.S. Cutler, et al., ^{177}Lu-labeled RGD-BBN heterodimeric peptide for targeting prostate carcinoma, *Nucl Med Commun* **34**, 2013, 909–914.

[5] J.C. Sanders, T. Kuwert, J. Hornegger and P. Ritt, Quantitative SPECT/CT imaging of ^{177}Lu with in vivo validation in patients undergoing peptide receptor radionuclide therapy, *Mol Imaging Biol* **17**, 2015, 909–914.

[6] Y. Dewaraja, E. Frey, G. Sgouros, A. Brill, P. Roberson, P. Zanzonico, et al., MIRD pamphlet no. 23: quantitative SPECT for patient-specific 3-dimensional dosimetry in internal radionuclide therapy, *J Nucl Med* **53**, 2012, 1310-1325.

[7] IAEA, Quantitative Nuclear Medicine Imaging: Concepts, Requirements and Methods, 2014, International Atomic Energy Agency.

[8] M. Ljungberg, A. Celler, M.W. Konijnenberg, K.F. Eckerman, Y.K. Dewaraja and G.K. Sjogreen, MIRD pamphlet no. 26: joint EANM/MIRD guidelines for quantitative ^{177}Lu SPECT applied for dosimetry of radiopharmaceutical therapy, *J Nucl Med* 98857,

201<s>5</s>6, 151-162.

[9] B.E. Zimmerman, D. Grosev, I. Buvat, M.A. Coca Perez, E.C. Frey, A. Green, et al., Multi-centre evaluation of accuracy and reproducibility of planar and SPECT image quantification: an IAEA phantom study, *Z Med Phys* **27**, 2017, 98–112.

[10] K. Willowson, D.L. Bailey and C. Baldock, Quantitative SPECT reconstruction using CT-derived corrections, *Phys Med Biol* **53**, 2008, 3099–3112.

[11] A. Delker, W.P. Fendler, C. Kratochwil, A. Brunegraf, A. Gosewisch, F.J. Gildehaus, et al., Dosimetry for ^{177}Lu-DKFZ-PSMA-617: a new radiopharmaceutical for the treatment of metastatic prostate cancer, *Eur J Nucl Med Mol Imaging* **43**, 2016, 42–51.

[12] J. Gustafsson, G. Brolin, M. Cox, M. Ljungberg, L. Johansson and K.S. Gleisner, Uncertainty propagation for SPECT/CT-based renal dosimetry in ^{177}Lu peptide receptor radionuclide therapy, *Phys Med Biol* **60**, 2015, 8329–8346.

[13] R. de Nijs, V. Lagerburg, T.L. Klausen and S. Holm, Improving quantitative dosimetry in ^{177}Lu-DOTATATE SPECT by energy window-based scatter corrections, *Nucl Med Commun* **35**, 2014, 522–533.

[14] M. Sandström, U. Garske, D. Granberg, A. Sundin and H. Lundqvist, Individualized dosimetry in patients undergoing therapy with ^{177}Lu-DOTA-D-Phe1-Tyr3-octreotate, *EJNMMI Phys* **37**, 2010, 212–225.

[15] E. Hippeläinen, M. Tenhunen, H. Mäenpää and A. Sohlberg, Quantitative accuracy of ^{177}Lu SPECT reconstruction using different compensation methods: phantom and patient studies, *EJNMMI Res* **6**, 2016, 16.

[16] M. D'Arienzo, M. Cazzato, M.L. Cozzella, M. Cox, M. D'Andrea, A. Fazio, et al., Gamma camera calibration and validation for quantitative SPECT imaging with ^{177}Lu, *Appl Radiat Isot* **112**, 2016, 156–164.

[17] C.F. Uribe, P.L. Esquinas, J. Tanguay, M. Gonzalez, E. Gaudin, J.-M. Beauregard, et al., Accuracy of ^{177}Lu activity quantification in SPECT imaging: a phantom study, *EJNMMI Phys* **4**, 2017, 2.

[18] G. Marin, B. Vanderlinden, I. Karfis, T. Guiot, Z. Wimana, P. Flamen, et al., Accuracy and precision assessment for activity quantification in individualized dosimetry of ^{177}Lu-DOTATATE therapy, *EJNMMI Phys* **4**, 2017, 7.

[19] J. Tran-Gia, M. Lassmann, T. Kuwert and P. Ritt, Quantitative <s>b</s>Bildgebung für die <s>d</s>Dosimetrie mit SPECT/CT, *Nuklearmediziner* **41**, 2018, 24–36.

[20] E. Grassi, F. Fioroni, V. Ferri, E. Mezzenga, M.A. Sarti, T. Paulus, et al., Quantitative comparison between the commercial software STRATOS® by Philips and a homemade software for voxel-dosimetry in radiopeptide therapy, *Physica Med* **31**, 2015, 72–79.

[21] W. Zhao, P.L. Esquinas, X. Hou, C.F. Uribe, M. Gonzalez, J.-M. Beauregard, et al., Determination of gamma camera calibration factors for quantitation of therapeutic radioisotopes, *EJNMMI Phys* **5**, 2018, 8.

[22] E. Mezzenga, V. D'Errico, M. D'Arienzo, L. Strigari, K. Panagiota, F. Matteucci, et al., Quantitative accuracy of ^{177}Lu SPECT imaging for molecular radiotherapy, *PLoS One* **12**, 2017, e0182888.

[23] M. D'Arienzo, M.L. Cozzella, A. Fazio, P. De Felice, G. Iaccarino, M. D'Andrea, et al., Quantitative ^{177}Lu SPECT imaging using advanced correction algorithms in non-reference geometry, *Physica Med* **32**, 2016, 1745–1752.

[24] M. Ljungberg and S.E. Strand, A Monte Carlo program for the simulation of scintillation camera characteristics, *Comput Methods Programs Biomed* **29**, 1989, 257–272.

[25] A.P. Robinson, J. Tipping, D.M. Cullen and D. Hamilton, The influence of triple energy window scatter correction on activity quantification for ^{177}Lu molecular radiotherapy, *Phys Med Biol* **61**, 2016, 5107–5121.

[26] B. He, R.L. Wahl, Y. Du, G. Sgouros, H. Jacene, I. Flinn, et al., Comparison of residence time estimation methods for radioimmunotherapy dosimetry and treatment planning: Monte Carlo simulation studies, *IEEE Trans Med Imaging* **27**, 2008, 521–530.

[27] E.C. Frey and B.M.W. Tsui, A new method for modeling the spatially-variant, object-dependent scatter response function in SPECT, *IEEE Nucl Sci Symp* **2**, 1996, 1082–1086.

[28] E.C. Frey and B.M.W. Tsui, Collimator-Detector response compensation in SPECT, In: H. Zaidi, (Ed), *Quantitative analysis in nuclear medicine imaging,* 2006, Springer, US; Boston, MA, 141–166.

[29] C.F. Uribe, P.L. Esquinas, M. Gonzalez and A. Celler, Characteristics of Bremsstrahlung emissions of ^{177}Lu, [188]Re, and ^{90}Y for SPECT/CT quantification in radionuclide therapy, *Physica Med* **32**, 2016, 691–700.

[30] G.C.A. Costa, D.A.B. Bonifacio, D. Sarrut, T. Cajgfinger and M. Bardies, Optimization of GATE simulations for whole-body planar scintigraphic acquisitions using the XCAT male phantom with ^{177}Lu-DOTATATE biokinetics in a Siemens Symbia T2, *Phys Med* **42**, 2017, <s>6</s>292-297.

[31] H.M. Hudson and R.S. Larkin, Accelerated image reconstruction using ordered subsets of projection data, *IEEE Trans Med Imaging* **13**, 1994, 601–609.

[32] L. Shao, R. Freifelder and J.S. Karp, Triple energy window scatter correction technique in PET, *IEEE Trans Med Imaging.* **13**, 1994, 641–648.

[33] M. Ljunberg, S.E. Strand and M.A. King, Monte Carlo calculation in nuclear medicine, 2013, CRC Press, Taylor & Francis Group; Boca Raton, FL.

[34] E. Grassi, F. Fioroni, S. Berenato, N. Patterson, V. Ferri, L. Braglia, et al., Effect of image registration on 3D absorbed dose calculations in ^{177}Lu-DOTATOC peptide receptor radionuclide therapy, *Physica Med* **45**, 2018, 177–185.

[35] NEMA, Performance measurement of positron emission tomography, 2001, National Electrical Manufacturers Association; Washington, D.C..

[36] A.H. Vija, E.G. Hawman and J.C. Engdahl, Analysis of a SPECT OSEM reconstruction method with 3D beam modeling and optional attenuation correction: phantom studies, In: *2003 IEEE Nuclear Science Symposium Conference Record (IEEE Cat No03CH37515),* 2003, 2662–2666.

[37] G.K.V. Schulthess, Molecular anatomic imaging: PET-CT and SPECT-CT integrated modality imaging, 2nd ed., 2007, Lippincott Williams & Wilkins; Philadelphia, USA.

[38] Y. Seo, K.H. Wong, M. Sun, B. Franc, R.A. Hawkins and B.H. Hasegawa, Calculation and validation of the use of effective attenuation coefficient for attenuation correction in In-111 SPECT, *Med Phys* **32**, 2005, 3628–3635.

[39] T.C. Lee, A.M. Alessio, R.M. Miyaoka and P.E. Kinahan, Morphology supporting function: attenuation correction for SPECT/CT, PET/CT, and PET/MR imaging, *Q J Nucl Med Mol Imaging* **60**, 2016, 25–39.

Appendix A. Supplementary data

The following are the Supplementary data to this article:

Multimedia Component 1

Supplementary Data 1

Highlights

- Dependency of ^{177}Lu SPECT calibration factors on phantom size.

- Influence of volume of interests on ^{177}Lu SPECT calibration factors.

- Effect of attenuation maps on ^{177}Lu SPECT calibration factor.

- ESSE performed better than TEW in simulations.

- Scatter energy windows are suggested for improved TEW scatter correction.

Queries and Answers

Query: Your article is registered as a regular item and is being processed for inclusion in a regular issue of the journal. If this is NOT correct and your article belongs to a Special Issue/Collection please contact s.hurren@elsevier.com immediately prior to returning your corrections.
Answer: this is a regular paper

Query: The author names have been tagged as given names and surnames (surnames are highlighted in teal color). Please confirm if they have been identified correctly.
Answer: Yes

Query: The country name has been inserted for the 'c', 'd' affiliation. Please check, and correct if necessary.
Answer: correct

Query: Have we correctly interpreted the following funding source(s) and country names you cited in your article: Helmholtz Graduate School of Environmental Health, Germany? /
Answer: